Measurement of Neutron Activation Cross Sections for Energies up to 40 MeV for Natural Samples of Mg, Si, Ca, V, Cr, Cu and Zn

Yoshitomo UWAMINO,

*Institute for Nuclear Study, University of Tokyo**

Hiroshi SUGITA, Yuhri KONDO
and Takashi NAKAMURA

*Cyclotron and Radioisotope Center, Tohoku University***

Received December 18, 1992
Revised May 6, 1993

The cross section measurements of 17 neutron induced reactions using an intense semi-monoenergetic neutron field were recently reported. Neutrons for energies up to 40 MeV were produced by a simple Be target system bombarded by protons of 9 different energies between 20 and 40 MeV.

Successively in this neutron field, we measured the cross sections of 15 reactions of $^{nat}Mg(n, Xnp)^{24}Na$, $^{nat}Si(n, Xn2p)^{27}Mg$, $^{nat}Si(n, Xnp)^{28}Al$, $^{nat}Si(n, Xnp)^{29}Al$, $^{nat}Ca(n, Xnp)^{42}K$, $^{nat}Ca(n, Xnp)^{43}K$, $^{nat}V(n, Xn2p)^{46}Sc$, $^{nat}V(n, Xn2p)^{47}Sc$, $^{nat}Cr(n, Xnp)^{52}V$, $^{nat}Cr(n, Xnp)^{53}V$, $^{nat}Cu(n, Xn2p)^{62m}Co$ ($T_{1/2}$=14 min), $^{nat}Zn(n, Xn2p)^{65}Ni$, $^{nat}Zn(n, Xnp)^{64}Cu$, $^{nat}Zn(n, Xnp)^{66}Cu$ and $^{nat}Zn(n, Xnp)^{68m}Cu$ ($T_{1/2}$=3.8 min) by irradiating natural samples of Mg, Si, Ca, V, Cr, Cu and Zn. The excitation functions of these reactions were obtained by using the least-squares fitting (LSF) of the cross-section values calculated with the ALICE/LIVERMORE82 code, and also by using the SAND-II and the NEUPAC unfolding codes with the initial guess values derived from the LSF results and empirical reference data.

***KEYWORDS:** experimental data, neutron activation cross sections, neutron reactions, neutrons, 40 MeV range, natural sample, semimonoenergetic neutron field, unfolding, magnesium, silicon, calcium, vanadium, chromium, copper, zinc*

I. INTRODUCTION

Activation cross sections for high energy neutrons are needed as basic data for neutron dosimetry, radiation safety and material damage studies, and for nuclear physics. The interest in the cross-section data of neutron energy above 20 MeV is now increasing and the related conference reports[1][2] and books [3][4] have recently been published. Those cross section data are, however, still very poor and no evaluated data file exists, since preparing a monoenergetic neutron source for activation experiment in this energy region presents some difficulties[5].

The authors recently published a paper[6] on the cross section measurements of 17 reactions of $^{23}Na(n, 2n)^{22}Na$, $^{27}Al(n, \alpha)^{24}Na$, $^{51}V(n, \alpha)^{48}Sc$, $^{51}V(n, p)^{51}Ti$, $^{50}Cr(n, 3n)^{48}Cr$, $^{50}Cr(n, 2n)^{49}Cr$, $^{55}Mn(n, p\alpha)^{51}Ti$, $^{55}Mn(n, 4n)^{52}Mn$, $^{55}Mn(n, 2n)^{54}Mn$, $^{63}Cu(n, 3n)^{61}Cu$, $^{63}Cu(n, 2n)^{62}Cu$, $^{65}Cu(n, p)^{65}Ni$, $^{64}Zn(n, t)^{62}Cu$, $^{64}Zn(n, 3n)^{62}Zn$, $^{64}Zn(n, 2n)^{63}Zn$, $^{197}Au(n, 4n)^{194}Au$ and $^{197}Au(n, 2n)^{196}Au$ using an intense semimonoenergetic neutron field[7] which has been established at the SF Cyclotron of the Institute for Nuclear Study, University of Tokyo. Neutrons for energies up to 40 MeV were pro-

* *Midori-cho, Tanashi-shi 188.*
** *Aoba, Aramaki, Aoba-ku, Sendai 980.*

duced by a simple Be target system bombarded by protons of 9 different energies between 20 and 40 MeV. Since the spectrum of this neutron field is not purely monoenergetic, that is, a high energy peak coming from the Be(p, n) reaction is broad and a low energy tail coming from the Be target and also from the coolant water exists, an unfolding technique is necessary for obtaining an excitation function from measured activation rates of irradiated samples[8]~[10].

Successively in this work, we measured the cross sections up to 40 MeV of 15 reactions of ^{nat}Mg(n, Xnp)^{24}Na, ^{nat}Si(n, $Xn2p$)^{27}Mg, ^{nat}Si(n, Xnp)^{28}Al, ^{nat}Si(n, Xnp)^{29}Al, ^{nat}Ca(n, Xnp)^{42}K, ^{nat}Ca(n, Xnp)^{43}K, ^{nat}V(n, $Xn2p$)^{46}Sc, ^{nat}V(n, $Xn2p$)^{47}Sc, ^{nat}Cr(n, Xnp)^{52}V, ^{nat}Cr(n, Xnp)^{53}V, ^{nat}Cu(n, $Xn2p$)^{62m}Co ($T_{1/2}$= 14 min), ^{nat}Zn(n, $Xn2p$)^{65}Ni, ^{nat}Zn(n, Xnp)^{64}Cu, ^{nat}Zn(n, Xnp)^{66}Cu and ^{nat}Zn(n, Xnp)^{68m}Cu ($T_{1/2}$=3.8 min) by irradiating natural samples of Mg, Si, Ca, V, Cr, Cu and Zn in this neutron field. The cross-sections of these reactions were calculated by the ALICE/LIVERMORE82 code[11], and they were adjusted to the measured reaction rates with the multi-parametric least-squares fitting (LSF). The LSF results were utilized as the initial guesses of two unfolding codes, SAND-II[12] and NEUPAC[13], which were used for the unfolding of the measured activation rates to excitation functions.

II. Neutron Field for Activation Experiment

Since a detailed description of the target system and of the neutron spectrum are given in a previous paper[7], they are described briefly here. Proton beams of energies at every 2.5 MeV between 20 and 40 MeV were impinged to 1-mm-thick (E_p=20 to 37.5 MeV) and 2-mm-thick (E_p=40 MeV) Be targets, which were backed by a water coolant. Protons lose part of their energy at the Be target and totally stop in the water coolant.

The neutrons produced in the forward direction by this target system were measured with a 51-mm-dia.×51-mm-long NE-213 scintillation counter placed at about 1.1 m from the target. Since the measured peak spectrum spread wider than the reality due to the energy resolution of the detection system, the measured spectrum of the peak energy region was replaced by the calculated spectrum of which peak area had been adjusted same as the measured one[7]. The neutron spectra are shown in **Fig. 1** with the errors indicated in vertical bars. The digits in the figures indicate the incident proton energies (E_p) and average peak energies. Since the Be target is not thin, a high-energy peak due to the ^{9}Be(p, n) reaction is not sharp. A low-energy tail coming from the Be target and the water beam stopper is present.

III. Measurement of Induced Radioactivity

The purity and the size of the irradiated samples are listed in **Table 1**. Since it is difficult to handle a metal Ca sample, a $CaCO_3$ sample was used instead. Oxygen and carbon nuclei in the sample produce radioactivities having much shorter half-lives than Ca, and this compound can be used without any problem. The other samples are all metals. The maximum size of the samples is 20 mm in diameter, and the flux depression of high-energy neutrons at the sample edge is estimated to be $<3\%$ in spite of their very sharp forward angular distribution[7].

The activation samples except silicon were irradiated by turns for 1 h at 20 cm from the Be target. The Si sample was irradiated for 20 min. These irradiations were repeated for 9 proton energies.

The irradiated samples were placed on a Ge detector for γ-ray spectrometry. Each sample was measured several times with suitable intervals. The obtained pulse-height spectra were analyzed by the KEI-11EF program[14] to get photo-peak areas. The peak detection efficiencies were calculated by a Monte Carlo code, PEAK[15], which can evaluate the self-absorption of γ-rays in a source disk. The accuracy of the PEAK code had been experimentally checked for the Ge de-

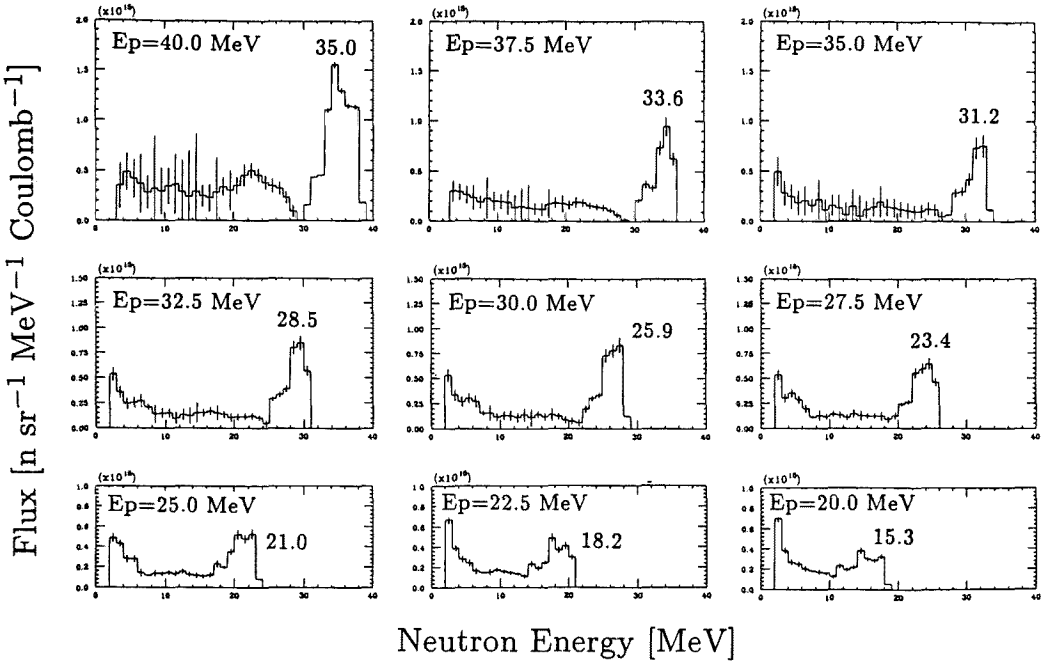

Fig. 1 Corrected neutron spectra of the irradiation fields

Table 1 Specification of the irradiated samples

Nuclide	Chemical form	Purity (%)	Size (mm)
Mg	Metal	99.99	20.0 dia.×2.0
Si	Metal	99.999	17.0 dia.×2.0
Ca	$CaCO_3$	99.999	20.0 dia.×2.0
V	Metal	99.7	5.0×5.0×5.0
Cr	Metal	99.99	5.0×5.0×5.0
Cu	Metal	99.99	20.0 dia.×1.0
Zn	Metal	99.9999	15.0 dia.×2.1

tector that was used and found to be of $<10\%$ error. The coincidence-summing corrections were performed by the SUMECC code[16]. Total detection efficiencies, which are necessary for the SUMECC code, were calculated by the PEAK code. The data of decay schemes were derived from Ref. (17).

IV. Calculation of Cross Sections

Since the neutron fields used in this activation experiment are not purely monoenergetic, excitation functions cannot be obtained directly, but can be obtained by using the unfolding method and the LSF method using the activation rates at 9 different semimonoenergetic neutron fields.

In LSF, considering the production of the relevant radionuclide through multi-reaction channels, initial values calculated by the ALICE/LIVERMORE82 code were adjusted to the measured reaction rates as shown in the following:

$$R=\sum_i\left[A_i-\sum_j\int_0^{E_{\max}}\sigma_j(E)\Phi_i(E)dE\right]^2, \quad (1)$$

$$\sigma_j(E)=k_j g_j(E), \quad (2)$$

where A_i: Activation rate at i'th neutron field
$g_j(E)$: Calculated excitation function by ALICE for j'th reaction channel
$\Phi_i(E)$: Neutron flux shown in Fig. 1.

By determining the k_j value to make R minimum, the excitation function $\Sigma_j\sigma_j(E)$ was obtained.

In the use of the revised nuclear evaporation code, ALICE/LIVERMORE82[11], the geometry-dependent hybrid model was selected for precompound decay, since this model generated the most consistent results with the experiment in the test calculations. The

default values recommended by the authors of the code were chosen most often in the calculation.

The measured reaction rates were converted into excitation functions by the unfolding codes, SAND-II[12] and NEUPAC[13]. The concept of the former code is the iterative perturbation method, and that of the latter is the variational principle, the so-called "J-1 method". These unfolding codes are usually used for neutron spectrum measurements by foil activations where the excitation functions of used foils are known. In contrast, in this work the neutron spectra were used as known input data, and unknown excitation functions were obtained.

These codes require an initial guess as input data, and it was obtained from the result of the LSF calculation and some empirical reference data as shown in **Table 2**. The initial guess of the $^{nat}Mg(n, Xnp)^{24}Na$ reaction, for example, was obtained from the IAEA curve of $^{24}Mg(n, p)$ cross section and the LSF result which were smoothly connected at 15 MeV.

The NEUPAC code evaluates the propagation of errors of initial guess values, neutron spectra, and reaction rates to the resultant excitation functions. Errors of the neutron spectra are about 10% in the peak region and about 30 to 50% in the low-energy tail as shown in Fig. 1, and errors of the activation rates are about 10%. The errors of the initial guess values are unknown. They were, however, set at 60%, since this value seemed to be adequate, that is, the results of the NEUPAC code adopting this value seemed to be reasonable with our experimental data and also with the empirical reference data. The errors of the initial guess values are most dominant on the propagated errors. Unfolded results are almost bound within the error band of the initial guess, and the fluctuations of the SAND-II results are usually larger than those of the NEUPAC results.

V. Results and Discussion

Fifteen reactions of which cross sections were measured are listed in Table 2. These $(n, XnYp)$-type reactions are the mixtures of several competing reactions which are also shown in Table 2, since natural samples used in this experiment contain more than one isotope.

The obtained cross section curves are shown in Figs. 2(a)~(o), where the results obtained by the unfolding processes performed by the SAND-II and the NEUPAC codes are shown in a thin zigzag solid line and a thin zigzag dotted line, respectively. The vertical bars attached on the NEUPAC results show errors estimated by this code. Results of the ALICE/LIVERMORE82 code were adjusted by the LSF and they are shown in a thin dashed line. If some reference data are available, they are also drawn in the same figure in a thick dashed line for ENDF-B/V[18], in a thick dash-dot line for JENDL-3[19], in a thick fine-dotted line for *IAEA Tech. Rep.* 273[3] and in circles for experimental values compiled by McLane, Dunford & Rose[4], which is the fourth edition of the *BNL*-325 and is here referred to as *BNL*-325. The cross section data calculated with the GNASH code by Yamamuro[20] for the $^{nat}Zn(n, Xnp)^{64}Cu$ and the $^{nat}Zn(n, Xnp)^{66}Cu$ reactions are also shown in a thin dash-dot line. The results and discussions are given separately for each reaction in the following.

(1) $^{nat}Mg(n, Xnp)^{24}Na$ (**Fig. 2**(a))

This reaction can be considered to be a mixture of $^{24}Mg(n, p)$, $^{25}Mg(n, d)$ and $^{26}Mg(n, t)$ as shown in Table 2. In this article the (n, t) reaction, for example, means a mixture of the (n, t), (n, nd) and $(n, 2np)$ reactions. The main channel of this reaction is $^{24}Mg(n, p)$ due to a large abundance of ^{24}Mg (78.99%), and a lower threshold energy (4.93 MeV) and a generally higher cross section value of the (n, p) reaction than those of other reactions[21]. The SAND-II and NEUPAC results show good agreement within errors, except an unreasonable oscillation in the SAND-II result above 30 MeV. The LSF result also shows good agreement with these two unfolded results, but its rising up region below 10 MeV is shifted to higher energy than the others, reflecting the ALICE result.

Table 2 Observed productions, competing reactions, threshold energies, natural abundances, sources of initial guesses for unfolding process and recommendations for best result

Production	Reaction	Threshold energy (MeV)	Natural abundance (%)	Source of unfolding initial guess	Recommendation for best result
Mg→^{24}Na	^{24}Mg(n,p)*	4.93	^{24}Mg 78.99	<15 MeV IAEA	<10 MeV NEUPAC
	^{25}Mg(n,d)	12.54	^{25}Mg 10.00	of ^{24}Mg(n,p)	>10 MeV LSF
	^{26}Mg(n,t)	15.24	^{26}Mg 11.01	>15 MeV LSF	
Si→^{27}Mg	^{28}Si$(n,2p)$†	13.89	^{28}Si 92.23	LSF	NEUPAC
	^{29}Si$(n,^3$He$)$†	14.66	^{29}Si 4.67		
	^{30}Si(n,α)*	4.34	^{30}Si 3.10		
Si→^{28}Al	^{28}Si(n,p)*	4.00		<16 MeV IAEA	NEUPAC
	^{29}Si(n,d)	10.46		of ^{28}Si(n,p)	
	^{30}Si(n,t)	14.94		>16 MeV LSF	
Si→^{29}Al	^{29}Si(n,p)*	3.00		LSF	SAND-II
	^{30}Si(n,d)†	11.66			
Ca→^{42}K	^{42}Ca(n,p)*	2.80	^{40}Ca 96.94	<12 MeV IAEA	NEUPAC
	^{43}Ca(n,d)†	8.64	^{42}Ca 0.647	of ^{42}Ca(n,p)	
	^{44}Ca(n,t)†	13.62	^{43}Ca 0.135	>12 MeV LSF	
	^{46}Ca$(n,2nt)$	31.81	^{44}Ca 2.09		
	^{48}Ca$(n,4nt)$	49.36	^{46}Ca 0.004		
			^{48}Ca 0.187		
Ca→^{43}K	^{43}Ca(n,p)*	1.06		LSF	see text
	^{44}Ca(n,d)†	10.17			
	^{46}Ca(n,nt)	21.97			
	^{48}Ca$(n,3nt)$	39.53			
V→^{46}Sc	^{50}V$(n,n\alpha)$†	10.09	^{50}V 0.25	LSF	LSF
	^{51}V$(n,2n\alpha)$*	21.35	^{51}V 99.75		
V→^{47}Sc	^{50}V(n,α)†	0 (Q=0.76)		LSF	LSF
	^{51}V$(n,n\alpha)$*	10.50			
Cr→^{52}V	^{52}Cr(n,p)*	3.26	^{50}Cr 4.35	<15 MeV IAEA	<15 MeV SAND-II
	^{53}Cr(n,d)	9.08	^{52}Cr 83.79	of ^{52}Cr(n,p)	>15 MeV LSF
	^{54}Cr(n,t)	12.60	^{53}Cr 9.50	>15 MeV LSF	
			^{54}Cr 2.36		
Cr→^{53}V	^{53}Cr(n,p)*	2.69		<15 MeV BNL	NEUPAC
	^{54}Cr(n,d)†	10.32		eye-guide of ^{53}Cr(n,p)	
				>15 MeV LSF	
Cu→^{62m}Co	^{63}Cu$(n,2p)$	10.85	^{63}Cu 69.2	<20 MeV IAEA	NEUPAC
$T_{1/2}$=14 min	^{65}Cu(n,α)*	0.21	^{65}Cu 30.8	of ^{65}Cu(n,α)	
				>20 MeV LSF	
Zn→^{65}Ni	^{66}Zn$(n,2p)$†	10.44	^{64}Zn 48.6	LSF	<20 MeV SAND-II
	^{67}Zn$(n,^3$He$)$	9.76	^{66}Zn 27.9		>20 MeV NEUPAC
	^{68}Zn(n,α)*	0 (Q=0.77)	^{67}Zn 4.10		
	^{70}Zn$(n,2n\alpha)$	15.15	^{68}Zn 18.8		
			^{70}Zn 0.62		
Zn→^{64}Cu	^{64}Zn(n,p)*	0 (Q=0.20)		<17 MeV IAEA	NEUPAC
	^{66}Zn(n,t)†	10.51		of ^{64}Zn(n,p)	
	^{67}Zn(n,nt)	17.67		>17 MeV LSF	
	^{68}Zn$(n,2nt)$	28.01			
	^{70}Zn$(n,4nt)$	43.92			
Zn→^{66}Cu	^{66}Zn(n,p)*	1.89		LSF	NEUPAC
	^{67}Zn(n,d)	6.79			
	^{68}Zn(n,t)†	10.78			
	^{70}Zn$(n,2nt)$	26.70			
Zn→^{68m}Cu	^{68}Zn(n,p)*	4.63		LSF	NEUPAC
$T_{1/2}$=3.8 min	^{70}Zn(n,t)	11.95			

* Dominant reaction; † Supplemental observed reaction.

In the peak region between 10 and 17 MeV, the LSF result gives the highest value and the SAND-II result gives the lowest. Our results are compared here with the $^{24}Mg(n, p)$ cross section values of IAEA, ENDF-B/V, JENDL-3 and BNL-325 which are multiplied by the natural abundance of ^{24}Mg. This comparison reveals that the NEUPAC result agrees well with these data in the rising up region below 10 MeV, and above 10 MeV the LSF result is the closest to these data. It is confirmed that the $^{24}Mg(n, p)$ reaction is dominant and contributions of other reactions are negligibly small.

(2) $^{nat}Si(n, Xn2p)^{27}Mg$ (**Fig. 2**(b))

The LSF was performed with the results of the ALICE calculations for the $^{28}Si(n, 2p)$, $^{29}Si(n, {}^3He)$ and $^{30}Si(n, \alpha)$ reactions. The SAND-II and NEUPAC results agree well each other within unfolded errors, except a strong decrease of the SAND-II result above 35 MeV. The LSF result is slightly larger below 20 MeV and smaller above 20 MeV than the two unfolded results. The excitation functions have a peak at about 15 MeV which corresponds to the $^{30}Si(n, \alpha)$ reaction and a swelling above 20 MeV. Our SAND-II and NEUPAC results are close to the IAEA data and lie in the middle of the scattered data of *BNL*-325. The swelling may be due to the $^{28}Si(n, 2p)$ reaction.

(3) $^{nat}Si(n, Xnp)^{28}Al$ (**Fig. 2**(c))

This reaction was considered to consist of $^{28}Si(n, p)$, $^{29}Si(n, d)$ and $^{30}Si(n, t)$. The $^{28}Si(n, p)$ reaction is dominant because of the large abundance of ^{28}Si (92.23%), the lower threshold energy (4.0 MeV), and generally higher cross section value of (n, p) reaction than the others. The SAND-II and NEUPAC results agreed within the unfolded errors, and they are also close to the LSF result, except its rising up region. The IAEA curve gives about 60% higher value at the peak than our unfolded results which agree with the lowest data of *BNL*-325.

(4) $^{nat}Si(n, Xnp)^{29}Al$ (**Fig. 2**(d))

This reaction was considered to be a mixture of the $^{29}Si(n, p)$ and the $^{30}Si(n, d)$ reac-

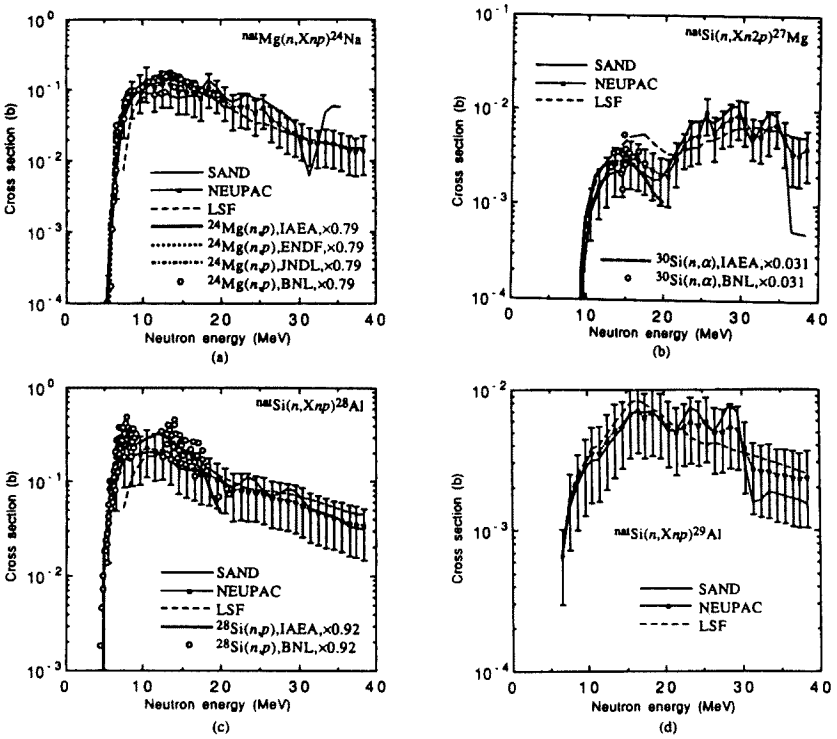

Fig. 2(a)～(d) Obtained excitation function curves

tions. The LSF, the SAND-II and the NEUPAC results are all in good agreement within unfolded errors. The excitation function has two peaks; a big peak around 16 MeV corresponds to the $^{29}Si(n, p)$ reaction and a small peak around 25 MeV to the $^{30}Si(n, d)$ reaction. No available reference data exist for this reaction.

(5) $^{nat}Ca(n, Xnp)^{42}K$ (**Fig. 2**(e))

The LSF was performed with the ALICE results of the $^{42}Ca(n, p)$, $^{43}Ca(n, d)$ and $^{44}Ca(n, t)$ reactions. Although the two unfolded results show oscillation, especially the SAND-II result, which may be caused by a statistical error of the measured activation rates, these three results are close each other, except a shift of LSF to higher energy above the threshold energy. The excitation functions have three peaks; the isolated lowest-energy peak around 15 MeV corresponds to the $^{42}Ca(n, p)$ reaction having a low threshold energy of 2.80 MeV. Our results are in good agreement below 15 MeV with the IAEA and the *BNL*-325 data of the $^{42}Ca(n, p)$ cross section.

(6) $^{nat}Ca(n, Xnp)^{43}K$ (**Fig. 2**(f))

The LSF result is larger below 15 MeV and smaller between 15 and 35 MeV than the SAND-II and the NEUPAC results which are close each other. Only at 15 MeV, our result is compared with the experimental data of the $^{43}Ca(n, p)$ and the $^{44}Ca(n, d)$ reactions by multiplying the natural abundances of ^{43}Ca and ^{44}Ca. The main component of the obtained excitation function is the $^{43}Ca(n, p)$ reaction cross section. The *BNL*-325 data of $^{43}Ca(n, p)$ are largely deviated, and it is therefore difficult to decide which cross section result is the best among our calculations.

(7) $^{nat}V(n, Xn2p)^{46}Sc$ (**Fig. 2**(g))

This reaction can be considered to be a sum of $^{50}V(n, n\alpha)$ and $^{51}V(n, 2n\alpha)$. The abundance of ^{50}V is very small (0.25%), and the latter reaction having threshold energy of 21.35 MeV may be dominant at higher energies. The three results of LSF, SAND-II and NEUPAC are very close altogether. Since

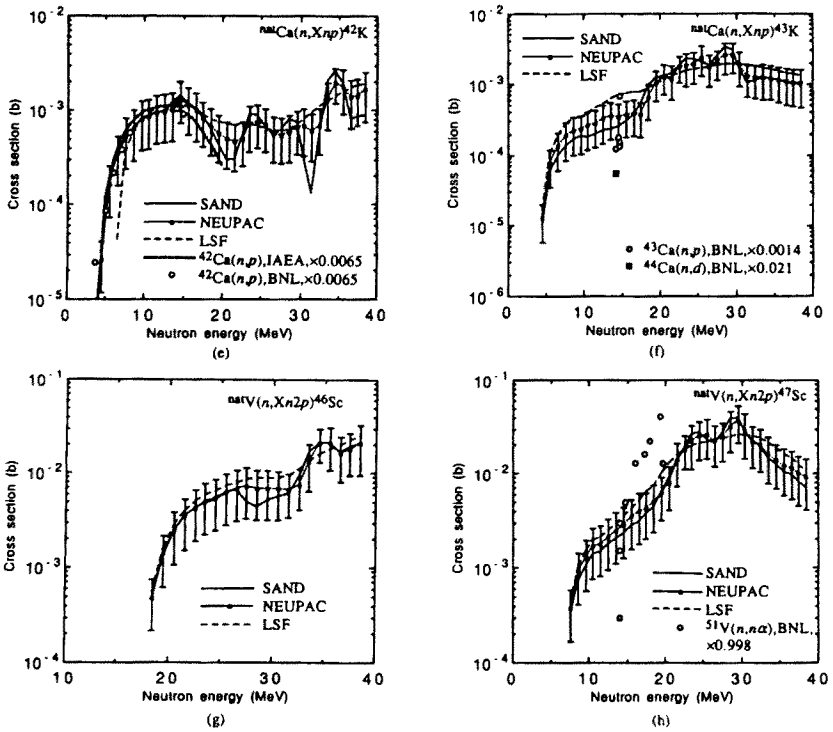

Fig. 2(e)~(h) Obtained excitation function curves

no experimental data exist, our cross section data are unique.

(8) $^{nat}V(n, Xn2p)^{47}Sc$ (**Fig. 2**(h))

This reaction is dominated at higher energies by the $^{51}V(n, n\alpha)$ reaction of which threshold energy is 10.50 MeV due to the small natural abundance of ^{50}V. The three results of LSF, SAND-II and NEUPAC are close altogether, but the LSF result gives the smoothest curve without small twin peaks between 20 and 30 MeV which are seen in the SAND-II and the NEUPAC results. Our results are compared with the *BNL*-325 data of the $^{51}V(n, n\alpha)$ reaction multiplied by the natural abundance of ^{51}V. The four cross section values at the neutron energies between 16.0 and 19.6 MeV given by Bormann *et al.*[22] are 3 to 5 times larger than our measurement.

(9) $^{nat}Cr(n, Xnp)^{52}V$ (**Fig. 2**(i))

Since ^{52}Cr has a large abundance of 83.79% and its (n, p) reaction has a low threshold energy of 3.26 MeV, this production is dominated by the $^{52}Cr(n, p)$ reaction. Excluding a rising up region of the LSF result, three results of LSF, SAND-II and NEUPAC show good agreement within the errors, although some oscillation can be seen in the SAND-II and NEUPAC results. Our results agree with the IAEA data of $^{52}Cr(n, p)$. In the energy region between 15 and 20 MeV, the LSF result is close to the higher values of *BNL*-325 data, while on the other hand, the SAND-II and NEUPAC results are close to the lower values of *BNL*-325 data. Contribution of the ^{53}Cr (n, d) reaction is negligibly small as seen in Fig. 2(i).

(10) $^{nat}Cr(n, Xnp)^{53}V$ (**Fig. 2**(j))

This reaction consists of two reactions of $^{53}Cr(n, p)$ and $^{54}Cr(n, d)$. Excluding a rising up region of the LSF result, our three results show good agreement within the errors. The unfolded results can be divided into a peak and a bump at a boundary of about 20 MeV. The peak around 15 MeV indicates good agreement with the *BNL*-325 data of ^{53}Cr (n, p) cross section multiplied by the natural abundance of ^{53}Cr. The small bump above 20 MeV might be a contribution of the ^{54}Cr

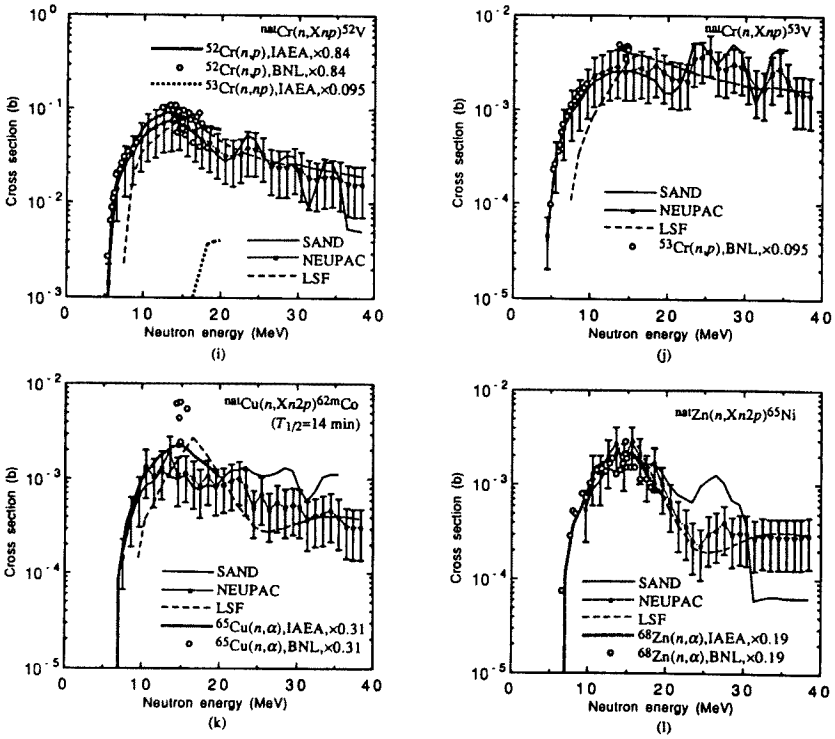

Fig. 2(i)～(l) Obtained excitation function curves

(n, d) reaction.

(11) $^{nat}Cu(n, Xn2p)^{62m}Co$ ($T_{1/2}$=14 min) (**Fig. 2**(k))

This reaction consists of two reactions of $^{63}Cu(n, 2p)$ and $^{65}Cu(n, \alpha)$. The results given by LSF, SAND-II and NEUPAC are slightly different each other. In the energy region below 15 MeV, the NEUPAC result shows good agreement with the IAEA data of ^{65}Cu (n, α) and we therefore consider that the NEUPAC result may be most appropriate.

(12) $^{nat}Zn(n, Xn2p)^{65}Ni$ (**Fig. 2**(l))

This reaction consists of three reactions of $^{66}Zn(n, 2p)$, $^{67}Zn(n, ^3He)$ and $^{68}Zn(n, \alpha)$. The three results of LSF, SAND-II and NEUPAC agree within the error below 20 MeV, but they show large discrepancy above 20 MeV. At a large peak below 20 MeV, the SAND-II result agrees well with the IAEA curve and the *BNL*-325 data of the $^{68}Zn(n, \alpha)$ cross section. The second small bump at about 25 MeV which are seen in SAND-II and NEUPAC might be due to the $^{66}Zn(n, 2p)$ reaction.

(13) $^{nat}Zn(n, Xnp)^{64}Cu$ (**Fig. 2**(m))

This reaction almost consists of two reactions of $^{64}Zn(n, p)$ and $^{66}Zn(n, t)$. The LSF result is higher than the unfolded results below 15 MeV and is very close to them above 15 MeV. The *BNL*-325 data of $^{64}Zn(n, p)$ are classified into two groups in the peak region between 5 and 15 MeV, the higher and the lower groups. The lower group agrees with our SAND-II and NEUPAC results, and the evaluated values of JENDL-3 and IAEA. The first peak below 20 MeV is certainly due to the $^{64}Zn(n, p)$ reaction from this comparison and the second peak above 20 MeV may be due to the $^{66}Zn(n, t)$ reaction. The ^{nat}Zn $(n, Xnp)^{64}Cu$ cross sections was calculated with the GNASH code by Yamamuro. His calculated result in Fig. 2(m) agrees with our results below 20 MeV, but gives about a factor of 3 higher values above 30 MeV.

(14) $^{nat}Zn(n, Xnp)^{66}Cu$ (**Fig. 2**(n))

This reaction consists of three reactions of $^{66}Zn(n, p)$, $^{67}Zn(n, d)$ and $^{68}Zn(n, t)$. Our three results show good agreement within

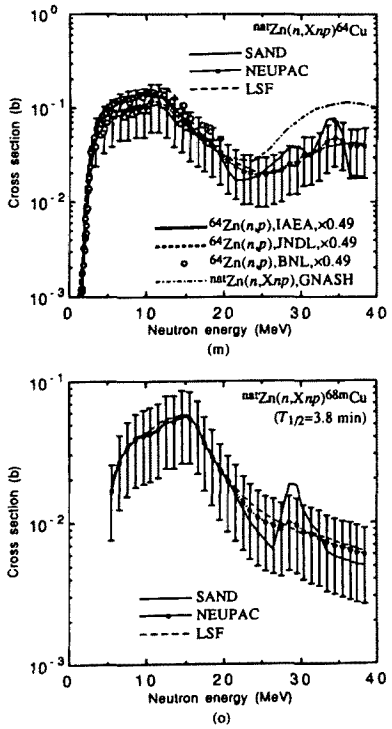

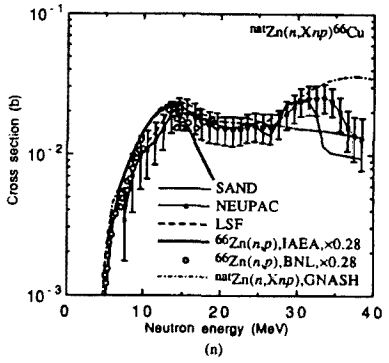

Fig. 2(m)~(o) Obtained excitation function curves

the error below 28 MeV. The peak below 20 MeV corresponds to ^{66}Zn(n, p) and our results indicate there a good agreement with the *BNL*-325 data. The IAEA curve is slightly higher below 12 MeV. The peak in the unfolded results around 33 MeV may be due to the ^{67}Zn(n, d) and the ^{68}Zn(n, t) reactions. The GNASH result by Yamamuro gives good agreement with our results below 33 MeV.

(15) ^{nat}Zn(n, Xnp)^{68m}Cu ($T_{1/2}$=3.8 min) (**Fig. 2**(o))

This reaction consists of two reactions of ^{68}Zn(n, p) and ^{70}Zn(n, t), but the former is the dominant reaction due to larger abundance of ^{68}Zn (18.8%) and low threshold energy (4.63 MeV) compared to the latter. Our three results are close each other, except a big bump of SAND-II around 30 MeV which may come from the statistical error of the measured reaction rate. No reference data exist for this reaction and our results are the first experimental data.

Three excitation functions were obtained for every reaction by using the LSF method, and the SAND-II and the NEUPAC unfolding codes. It depends on reactions what method seems to give the most reasonable result, and recommended methods giving the best results are listed in Table 2.

The numerical data will be sent on request.

VI. SUMMARY

The excitation functions of 15 activation reactions were obtained for neutron energies up to 40 MeV by unfolding the activation rates measured at 9 different semimonoenergetic neutron fields, succeeding to our previous paper which gave 17 activation reaction cross sections. Although the estimated error of our results is not small for many reactions, we gave useful experimental cross-section data for these activation reactions above 20 MeV. Our results are the first data for three activation reactions.

ACKNOWLEDGMENT

The authors are very grateful to Dr. M. Imamura, Dr. S. Shibata, Mr. T. Ohkubo, Mr. S. Sato and the SF cyclotron machine group for their devoted help during the neutron irradiations. The Staffs of the computer room of the Institute for Nuclear Study must also be appreciated. This work was financially supported by a Grant-in-Aid for Cooperative Research of the Japanese Ministry of Education, Science and Culture.

—REFERENCES—

(1) *Proc. Spec. Mtg. on Neutron Cross Section Standards for the Energy Region above 20 MeV, NEANDC*-305'U', (1991), The. Svedberg Lab., Uppsala, Sweden.

(2) *Proc. Spec. Mtg. on High Nuclear Data, INDC (JPN)*-158/L, (ed. FUKAHORI, T.), *JAERI-M* 92-039, (1991).

(3) MANOKHIN, V.N., PASHCHENKO, A.B., PLYASKIN, V.I., BYCHKOV, V.M., PRONYAEV, V.G.: Activation cross-sections induced by fast neutrons, *Handbook on Nuclear Activation Data, IAEA Tech. Rep. Ser.* No. 273, (1987).

(4) MCLANE, V., DUNFORD, C.L., ROSE, P.F.: Neutron cross section curves, *Neutron Cross Sections*, Vol. 2, (1988), Academic Press, New York.

(5) BAYHURST, B.P., GILMORE, J.S., PRESTWOOD, R.J., WILHELMY, J.B., NELSON, J., ERKKILA, B.H., HARDEKOPF, R.A.: *Phys. Rev.*, C12, 451 (1975).

(6) UWAMINO, Y., SUGITA, H., KONDO, Y., NAKAMURA, T.: *Nucl. Sci. Eng.*, 111, 391 (1992).

(7) UWAMINO, Y., OHKUBO, T., TORII, A., NAKAMURA, T.: *Nucl. Instrum. Methods*, A271, 546 (1988).

(8) SMITH, D.L.: A least-squares method for deriving reaction differential cross-section information from measurements performed in diverse neutron fields, *ANL/NDM*-77, (1982).

(9) JANCZYSZYN, J.: An activation method of fast neutron excitation function determination, *Rep. INT* 190/I, (1985), Inst. of Phys. and Nucl. Tech., Cracow.

(10) WÖLFLE, R., SUDÁR, S., QAIM, S.M.: *Nucl. Sci. Eng.*, 91, 162 (1985).

(11) BLANN, M., BISPLINGHOFF, J.: Code ALICE/LIVERMORE 82, *UCID* 19614, (1983).

(12) MCELROY, W.N., BERG, S., CROCKETT, T., HAWKINS, R.G.: A computer-automated iterative method for neutron flux spectra determination by foil activation—A study of the iterative method, Vol. 1; BERG, S., MCELROY,

W.N.: —SAND II and associated codes, Vol. 2, *AFWL-TR*-67-41, (1967).

(13) TANIGUCHI, T., UEDA, N., NAKAZAWA, M., SEKIGUCHI, A.: Neutron unfolding package code 'NEUPAC-83', *NEUT Res. Rep.* 83-10, (in Japanese), Univ. of Tokyo, Dept. Nucl. Eng., (1984).

(14) KOMURA, K.: A computer program for the analysis of gamma-ray spectrum; Concerning the background subtraction, *INS-TCH-9*, (in Japanese), Univ. of Tokyo (1974).

(15) NAKAMURA, T., SUZUKI, T.: *Nucl. Instrum. Methods*, **205**, 211 (1983).

(16) TORII, A., UWAMINO, Y., NAKAMURA, T.: Computer codes for activation data analysis, coincidence summing correction code; SUMECC and decay correction code; DECFIT, *INS-T*-468, (in Japanese), Univ. of Tokyo (1987).

(17) "*Table of Isotopes*", (7th ed.), (LEDERER, C.M., SHIRLEY, V.S., eds.), (1978), John Wiley and Sons, New York.

(18) ENDF/B summary documentation, *BNL-NCS*-17541 (*ENDF*-201), (3rd ed.), (ENDF/B-V), (1979).

(19) NAKAZAWA, M., KOBAYASHI, K., IWASAKI, S., IGUCHI, T., SAKURAI, K., IKEDA, Y., NAKAGAWA, T.: JENDL dosimetry file, *JAERI* 1325, (1992).

(20) YAMAMURO, N.: A nuclear cross section calculation system with simplified input format version II (SINCROS-II), *JAERI-M* 90-006, (1990).

(21) QAIM, S.M., WU, C.H., WÖLFLE, R.: *Nucl. Phys.*, A, **410**, 421 (1983).

(22) BORMANN, M., CIERJACKS, S., LANGKAU, R., NEUERT, H.: *Z. Phys.*, **166**, 477 (1962).